COVID-19 progression and convalescence in common variable immunodeficiency patients shows incomplete adaptive responses and persistent inflammasome activation

Javier Rodríguez-Ubreva
Josep Carreras Research Institute (IJC) https://orcid.org/0000-0003-4707-4536
Louis-Francois Handfield
Wellcome Sanger Institute
Baerbel Keller
University Medical Center and University of Freiburg
Laura Ciudad
Josep Carreras Leukaemia Research Institute (IJC)
Carlos de la Calle-Fabregat
Josep Carreras ResearchInstitute (IJC) https://orcid.org/0000-0002-3026-3069
Gerard Godoy-Tena
Josep Carreras Research Institute (IJC) https://orcid.org/0000-0003-3832-5794
Josep Calafell-Segura
Josep Carreras Research Institute (IJC) https://orcid.org/0000-0002-0173-8221
Eduardo Andrés-León
CSIC https://orcid.org/0000-0002-0621-9914
Regina Hoo
Nanyang Technological University
Tarryn Porter
Wellcome Sanger Institute
Elena Prigmore
Wellcome Trust Sanger Institute https://orcid.org/0000-0001-8870-0316
Maike Hofmann
University Hospital Freiburg https://orcid.org/0000-0001-8410-8833
Annegrit Decker
University Hospital Freiburg
Javier Martín
Institute of Parasitology and Biomedicine López Neyra, Spanish National Research Council
https://orcid.org/0000-0002-2202-0622
Klaus Warnatz

University Medical Centre Freiburg https://orcid.org/0000-0002-1172-865X

Roser Vento-Tormo

Wellcome Sanger Institute https://orcid.org/0000-0002-9870-8474

Esteban Ballestar (**eballestar@carrerasresearch.org**)

Josep Carreras Research Institute (IJC) https://orcid.org/0000-0002-1400-2440

Article

Keywords:

Posted Date: November 14th, 2022

DOI: https://doi.org/10.21203/rs.3.rs-2246352/v1

Abstract

Patients with common variable immunodeficiency (CVID), the most prevalent symptomatic primary immunodeficiency, are characterized by hypogammaglobulinemia, poorly protective vaccine titers and increased susceptibility to infections. New pathogens such as the severe acute respiratory syndrome coronavirus 2 (SARS-CoV-2), the causative agent of coronavirus disease 2019 (COVID-19), might constitute a particular threat to these immunocompromised patients since many of them experience a slower recovery and do not achieve full response to SARS-CoV-2 vaccines. To define the molecular basis of the altered immune responses caused by SARS-CoV-2 infection in CVID patients, we generated longitudinal single-cell datasets of peripheral blood immune cells along viral infection and recovery. We sampled the same individuals before, during and after SARS-CoV-2 infection to model their specific immune response dynamics while removing donor variability. We observed that COVID-19 CVID patients show defective canonical NF-κB pathway activation and dysregulated expression of BCR-related genes in naïve B cells, as well as enhanced cytotoxic activity but incomplete cytokine response in NK and T cells. Moreover, monocytes from COVID-19 CVID patients show persistent activation of several inflammasome-related genes, including the pyrin and NLRC4 inflammasomes. Our results shed light on the molecular basis of the prolonged clinical manifestations observed in these immunodeficient patients upon SARS-CoV-2 infection, which might illuminate the development of tailored treatments for COVID-19 CVID patients.

Introduction

Severe acute respiratory syndrome coronavirus 2 (SARS-CoV-2), the causative agent of coronavirus disease 2019 (COVID-19), constitutes an unprecedented threat to public health worldwide (https://covid19.who.int/). Although many COVID-19 patients are asymptomatic or experience mild symptoms, some patients experience hyperinflammatory responses that lead to severe disease that can evolve to severe lung dysfunction, multiorgan system failure and death [1]. In addition, persistent and often debilitating sequelae are increasingly recognized in convalescent individuals [2].

In relation to the particular immune responses mounted by the host upon SARS-CoV-2 infection, a fast induction of SARS-CoV-2-specific CD4+ T cells in acute infection has been associated with a mild COVID-19 course and a rapid viral clearance [3], whereas the lack of these specific CD4+ T cells was associated with severe COVID-19 [4,5]. Moreover, SARS-CoV-2-specific CD8+ T cell responses can develop rapidly during acute COVID-19, and the presence of these specific CD8+ T cells has been associated with better COVID-19 outcomes [5,6]. Regarding the humoral response, it has been shown a rapid generation of B cell memory during SARS-CoV-2 infection and convalescence [7], being the evolution of memory B cell responses consistent with antigen persistence [8]. In addition, SARS-CoV-2 neutralizing antibodies are produced by B cells with a wide range of heavy chain and light chain V genes [9]. On the other hand, HLA-$DR^{hi}CD11c^{hi}$ inflammatory monocytes with an interferon-stimulated gene (ISG) signature are elevated in mild COVID-19, whereas severe COVID-19 are marked by occurrence of neutrophil precursors,

dysfunctional mature neutrophils, and HLA-DR^{lo} monocytes [10]. Therefore, effective immune responses against SARS-CoV-2 require that the host's immune system provides a balanced and coordinated response involving both innate and adaptive immune systems [11,12].

In that context, patients with inborn errors of immunity (IEI) and, more specifically, patients with primary antibody deficiencies (PADs) may be exceptionally informative regarding the capacity of an altered immune system to mount a proper response against this viral infection, and may help to better understand the potential effects of a reduced antibody response during SARS-CoV-2 viral infection and resolution. Common variable immunodeficiency (CVID), the most common symptomatic PAD [13], is characterized by hypogammaglobulinemia and poorly protective vaccine titers. Most CVID patients have recurrent severe infections, whereas a substantial proportion develop autoimmune and inflammatory features [14,15]. Beside the classic defining antibody deficiency and B cell abnormalities, alterations of other immune compartments, including T cells and myeloid cells, have been described in CVID patients [16–19].

The course and outcome of SARS-CoV-2 infection among patients with CVID in comparison with the general population has been a matter of debate. For instance, several studies have reported a benign course of this particular viral infection in CVID patients [20–23], whereas other studies found high mortality rates among IEI patients including CVID patients [24], increased risk for severe COVID-19 in CVID patients with underlying chronic lung disease [25], or increased risks of both first infection and re-infection with SARS-CoV-2 among CVID individuals [26]. However, none of those studies have investigated in depth the dynamic responses mounted by these patients upon SARS-CoV-2 infection on a single-cell level.

Here, we performed a longitudinal study of peripheral blood samples from five CVID patients collected before, during and after SARS-CoV-2 infection using single-cell technology to compare the responses during viral infection and recovery of these patients in comparison with a healthy control cohort [27]. Our single-cell transcriptomic analysis shows that naïve B cells from COVID-19 CVID patients display an impaired canonical NF-κB pathway activation and a dysregulated expression of BCR-related genes. In addition, NK and T cells from these patients preserve their cytotoxic activity but show a reduced cytokine response. Finally, we find a persistent activation of several inflammasome-related genes in monocytes, together with an impaired upregulation of anti-inflammatory genes.

Our findings have important implications for understanding the *in vivo* transcriptional dysregulation in these immunodeficient patients upon an immunological challenge and the effect of a suboptimal antibody response on the general immune homeostasis in the context of SARS-CoV-2 infection and subsequent recovery. Furthermore, they may give insights into why CVID patients show prolonged clinical manifestations and viral positivity and the risk of these individuals to recurrent SARS-CoV-2 infections.

Results

Single-cell transcriptional profiling reveals a persistent type I IFN signature in COVID-19 CVID patients

We isolated paired samples of peripheral blood mononuclear cells (PBMCs) from five CVID patients at three distinct stages of the SARS-CoV-2 infection: 1) baseline, before viral infection, 2) progression, during viral infection, and 3) convalescence, once the viral infection had been resolved and the patient was PCR negative (Figure 1a). All collected CVID patients were under regular immunoglobulin replacement therapy and displayed only mild symptoms during SARS-CoV-2 infection (for detailed patient description see Supplementary Table 1). We profiled a total of 116,958 single-cell transcriptomes of isolated immune cells from the CVID cohort (Supplementary Table 2).

In addition, we processed and integrated publicly available single-cell RNA sequencing (scRNA-seq) datasets of PBMCs from a cohort of individuals without any known primary or secondary immunodeficiency (control cohort), who were either negative or positive for SARS-CoV-2 [27]. This control cohort included both non-CVID COVID-19 patients with mild symptoms (similar to patients in the CVID cohort) or severe symptoms (as a reference of a higher COVID-19-associated immune dysregulation). As in our CVID cohort, samples were classified in three stages: 1) baseline (48,517 cells), 2) progression (46,102 cells), and 3) convalescence (48,187 cells). Samples from the control cohort were selected to match in sex, age and time of sample collection after symptoms onset with our cohort of CVID patients (Supplementary Table 1). In addition, we integrated our data with 95,548 cells from 24 control individuals obtained from an additional publicly available scRNA-seq dataset of PBMCs to contextualize our analyses with previous work in that area that processed samples in a similar way to ours [28].

Our single-cell analysis transcriptomics census allowed us to identify several immune cell compartments at high resolution (Figure 1b): B cells, including naïve B cells, un-switched memory B cells, switched memory B cells, $CD21^{low}$ B cells and plasma cells (PCs); T cells, including naïve $CD4^+$ T cells, effector memory $CD4^+$ T ($CD4^+$ T_{EM}) cells, central memory $CD4^+$ T ($CD4^+$ T_{CM}) cells, effector $CD4^+$ T cells ($CD4^+$ T_{Eff}), naïve $CD8^+$ T cells, effector memory $CD8^+$ T ($CD8^+$ T_{EM}) cells, effector $CD8^+$ T ($CD8^+$ T_{Eff}) cells and cycling T ($T_{cycling}$) cells among others; Natural killer (NK) cells, including $CD56^{high}$ NK cells and $CD16^{high}$ NK cells; Myeloid cells, including classical, intermediate and non-classical monocytes, as well as conventional dendritic cells (cDC) and plasmacytoid dendritic cells (pDCs). All subsets have a good representation of the patients (Suppl. Table 3).

After immune cell subsets annotation, we analyzed the general response mediated by the interferon (IFN) proteins, which play a crucial role in the immune activity against viruses and other pathogens [29–31]. The inspection of well represented cell populations showed an increased type I IFN response during SARS-CoV-2 infection in all populations of both controls and CVID patients when compared to baseline (Figure 1c). However, in contrast to COVID-19 controls, type I IFN response was maintained at the convalescence stage in CVID patients in most cell subsets with the exception of monocytes.

Dysfunctional B cell receptor and NF-κB signaling pathways in COVID-19 CVID patients

The second line of defense against SARS-CoV-2 that we investigated addresses the humoral response. CVID patients are characterized by profound defects in humoral and B-cell-mediated immune responses.

Consistent with this knowledge, only one patient had detectable SARS-CoV-2 specific IgG antibodies and none of the patients produced specific IgA after COVID-19 (Supp. Table 1). Our scRNA-seq analysis allowed us to identify several B cell subsets in the three CVID patients with B cells (Figure 2a and Supp. Figure 1a). As expected for CVID patient samples [32], both switched memory B cells and PCs are underrepresented (Supplementary Table 3). For this reason, we focused our analyses on the transcriptional alterations of naïve B cells upon SARS-CoV2 infection, whose activation and differentiation gives rise to the aforementioned B cell subsets altered in CVID patients. Importantly, given that only a minor fraction of B cells might generate SARS-CoV-2 specific responses, we investigated global alterations in B cells which reflect not only a virus antigen specific response but also general immune stimulation of B cells via TLR and cytokines. Interestingly, our results showed that the naïve B cell compartment of the inspected COVID-19 CVID patients presented a dysregulated expression of several target genes of the canonical nuclear factor of κ light chain (NF-κB) pathway, including *CCL3*, *IL6*, *TNF*, *CD69*, *CD83, NFKBIA* and *EGR1* among others at progression and convalescence (Figure 2b). In this regard, we observed that the canonical NF-κB pathway displayed a significant activation upon SARS-CoV-2 infection only in control individuals and not in CVID patients (Figure 2c). Specifically, the p50 and p65 subunits displayed a significantly higher activity in both mild and severe COVID-19 controls at convalescence, which was only observed in severe COVID-19 controls at the progression stage. Interestingly, no significant activity of any of these subunits was detected at progression nor convalescence in CVID patients (Figure 2c). Conversely, we observed a significantly higher activity of the NF-κB inhibitor IκBα (*NFKBIA*) in COVID-19 CVID patients (Figure 2c), which is in line with the impaired activation of the NF-κB pathway observed in the immunodeficient patients. $CD21^{low}$ B cells have been previously described to display profound dysregulation of the canonical NF-κB pathway in CVID patients [33]. In our data, $CD21^{low}$ B cells constitute a separate cluster from naïve B cells (Figure 2a and Supp. Figures 1b and 1c), suggesting that the defective activation of the NF-κB pathway observed in the naïve B cell compartment is not a consequence of the presence of expanded $CD21^{low}$ B cells within the naïve B cell cluster.

In addition, we observed that the hypoxia-inducible factor 1-alpha (HIF-1α) transcription factor (TF), which might affect B cell function and induce B cell abnormalities in COVID-19 patients [34,35], showed a significantly higher activity at both progression and convalescence in naïve B cells of COVID-19 CVID patients (Figure 2c), despite the previously described impaired HIF-1α upregulation in CVID patients upon BCR *in vitro* stimulation [36]. Moreover, inflammation-related genes, such as *IL1B*, *IL6, LTA* and *TNF,* showed an impaired upregulation in naïve B cells of CVID individuals during SARS-CoV-2 infection compared with COVID-19 controls (Supp. Figure 1e).

Furthermore, we performed gene ontology (GO) analysis on naïve B cells and observed a higher enrichment in GO categories related to B cell activation and regulation of the B cell receptor (BCR) signaling pathway in COVID-19 CVID patients compared with COVID-19 controls (Figure 2d). Hence, we inspected the expression of BCR-related genes along the viral infection. We found a higher and persistent transcriptional upregulation of several genes encoding members of the BCR signaling pathway, both

activators and repressors, in the naïve B cell compartment of COVID-19 CVID patients compared with COVID-19 controls (Figure 2e and Supp. Figure 1d). This upregulation included BCR signaling pathway activator genes such as *CD19*, *CD81*, *CD79B*, *BTK* and *BLNK*, and also BCR inhibitory genes such as *PTPN6* (which encodes the tyrosine phosphatase SHP-1), *CD22* and *CD72* (Figure 2e).

Following the observation of a dysregulated BCR signaling, we analyzed the BCR repertoires of naïve B cells in our dataset. The inspection of the dynamics of the VDJ usage upon SARS-CoV-2 infection indicates that the proportion of B cells expressing the *IGHV3-53* gene, which has been described as the most frequently used IGHV gene among SARS-CoV-2 neutralizing antibodies [37,38], was increased in COVID-19 controls in contrast to COVID-19 CVID patients at both progression and convalescence stages (Figure 2f). Similar profiles were observed for the IGHV gene usage of other SARS-CoV-2 spike-targeting antibodies [27,37], such as *IGHV1-46, IGHV3-23 or IGHV5-51* (Figure 2f).

Altogether, we show that during SARS-CoV-2 infection, naïve B cells from CVID patients show a dysregulated expression of several components of the BCR signaling pathway, as well as a sustained impairment of NF-κB pathway activation, which might have a negative impact on the proper expression of relevant molecules involved in B cell responses.

Preserved and enhanced cytotoxicity but reduced cytokine responses in COVID-19 CVID NK and T cells

We next focused on the NK and T cell compartments (Figure 3a and Supp. Figure 2a) which also play key roles during SARS-CoV-2 infection [39–41]. $CD16^{high}$ NK cells, the most abundant subset of NK cells in our data, showed a significant enrichment in several GO categories related to NK cell cytotoxicity in CVID patients at the progression stage (Figure 3b). In line with this result, *GZMB*, *PRF1*, *GZMA* and *NKG7* - all of them relevant genes for cytotoxic activity - were upregulated in the $CD16^{high}$ NK cells of CVID patients during the infection and, to a lesser extent, in mild but not in severe COVID-19 individuals (Supp. Figure 2b). Interestingly, unlike in control individuals, the expression of these cytotoxic genes was maintained in CVID patients at the convalescence stage. Similarly, the minor $CD56^{high}$ NK cluster also showed that those cytotoxic genes were mainly upregulated in CVID patients compared with controls upon SARS-CoV-2 infection (Supp. Figure 2b).This higher and persistent cytotoxic activity in the NK compartment of COVID-19 CVID patient was also confirmed when we expanded the analysis to a higher number of cytotoxicity-related genes (see Methods) and calculated a cytotoxic score (Figure 3c). Additionally, both NK subsets presented an upregulation of IFN-γ and tumor necrosis factor alpha (TNF-α) coding genes in control individuals during infection, and even at a higher extent at the convalescence stage, but this upregulation was not observed in CVID patients (Figure 3d).

In addition, the aforementioned lytic-associated genes *GZMB*, *PRF1*, *GZMA* and *NKG7* were also upregulated in $CD8^+$ T_{Eff} cells and $CD8^+$ T_{EM} cells especially in of CVID patients during viral infection, whereas such upregulation was not so evident in COVID-19 controls (Supp. Figure 2b). Similarly to NK cells, we found a more persistent cytotoxic activity in the CD8+ T cell compartment of COVID-19 CVID patients that was not observed in COVID-19 controls (Figure 3c). In addition, we found a pronounced

upregulation of IFN-γ and TNF-α coding genes in $CD8^+$ T_{Eff} and $CD8^+$ T_{EM} cells of control individuals upon SARS-CoV-2 infection, especially remarked in the convalescence stage, which was not detected in CVID patients at the same stages (Figure 3d).

Multiple $CD4^+$ T cell subsets, including naïve $CD4^+$ T cells, $CD4^+$ T_{EM} cells, $CD4^+$ T_{CM} cells and $CD4^+$ T_{Eff} cells, showed upregulation of the TNF-α coding gene at the convalescence stage in control individuals (Figure 3e). In contrast, this upregulation was impaired in the distinct CD4+ T cell subsets of COVID-19 CVID patients (Figure 3e). The defective activation of CD4+ T cells in COVID-19 CVID patients was also observed for CD40L, whose transcriptional upregulation took place in $CD4^+$ T_{CM} cells of COVID-19 control individuals upon SARS-CoV-2 infection but not in COVID-19 CVID patients (Figure 3e).

All these results indicate that the NK and T cell compartments of COVID-19 CVID patients show incomplete antiviral immune responses with impaired gene expression of IFN-γ and TNF-α, as well as CD40L in the case of $CD4^+$ T_{CM} cells. On the contrary, NK and cytotoxic T cells from COVID-19 CVID patients display a higher activation state, expressing high levels of cytotoxic genes during SARS-CoV-2 infection, that are also maintained at convalescence.

Next, we performed TCR analysis. The highest level of T cell clonal expansion was observed in $CD8^+$ T_{EM} cells, $CD8^+$ T_{Eff} cells, $CD4^+$ CTL cells and $T_{cycling}$ cells (Supp. Figure 2c). The inspection of $CD4^+$ CTL cells showed that most of the expanded clones were already present in CVID patients prior to viral infection, whereas $CD8^+$ T_{EM} cells and specially $CD8^+$ T_{Eff} cells and $T_{prolif.}$ cells showed strong clonal expansion during progression and convalescence stages (Supp. Figure 2c). In contrast, MAIT cells, T_{DN} cells, as well as the different subsets of CD4 T cells, including naïve CD4+ T cells, $CD4^+$ T_{EM}, $CD4^+$ T_{CM}, $CD4^+$ T_{Eff} and T_{reg} cells, showed only a modest clonal expansion at progression and convalescence stages (Supp. Figure 2c). As expected, within the NK and $T_{\gamma\delta}$ cell clusters, only a small fraction of cells displayed a productive TCR chain, which may derive from cytotoxic T cells co-clustering with NK and $T_{\gamma\delta}$ cells.

Persistent activation of inflammasome genes in COVID-19 CVID monocytes

COVID-19 patients display functional and phenotypic alterations in monocytes [42–44]. Hence, we analyzed the three main subsets of monocytes (classical, intermediate and non-classical monocytes) during SARS-CoV-2 infection and recovery (Figure 4a and Supp. Figure 3a). Baseline vs progression or convalescence comparisons indicated that GO categories related to inflammasome complex assembly, pyroptosis and IL-1β production were more enriched in monocytes from COVID-19 CVID patients compared with those from COVID-19 control individuals (Figure 4b and Supp. Figure 3b). Interestingly, the three monocyte subsets displayed significant upregulation of genes that encode members of distinct inflammasome complexes in COVID-19 CVID patients. The inspection of several inflammasome sensor genes showed that the *AIM2* gene was upregulated upon SARS-CoV-2 infection in both CVID patients and control individuals regardless of disease severity. In contrast, we detected a specific and significant upregulation of the *NLRC4* gene (NLRC4 inflammasome) and the *MEFV* gene (pyrin inflammasome) during infection in

COVID-19 CVID patients that was not observed in control individuals (Figure 4c and Supp. Figure 3c). In line with this, the expression of many inflammasome-related genes was increased upon SARS-CoV-2 infection and was also maintained during convalescence in CVID patients unlike control individuals. For instance, *CASP1*, *CARD8*, *CARD16*, *PYCARD* and *GSDMD* genes were highly expressed at both progression and convalescence stages in COVID-19 CVID patients, whereas such persistent upregulation was not observed in mild or severe COVID-19 control individuals (Fig 4c and Supp. Figure 3c).

Next, we analyzed the gene expression of the toll-like receptors TLR7 and TLR8, which are sensors of single stranded RNAs, as the SARS-CoV-2 genome. We observed that these two receptors were significantly upregulated in COVID-19 CVID patients upon SARS-CoV-2 infection in the three subsets of monocytes, in contrast to COVID-19 controls (mild or severe) where the upregulation occurs only in intermediate monocytes (Figure 4d). Furthermore, we observed that TLR7 and TLR8 gene upregulation persisted only in COVID-19 CVID patients at the convalescence stage in comparison with COVID-19 controls (Figure 4d).

Finally, we analyzed the expression of several anti-inflammatory genes in the three monocyte subsets upon SARS-CoV-2 infection. *IL10*, *ARG1*, *SOCS3*, *PPARG*, *ADM* and *CD63* genes were upregulated upon SARS-CoV-2 infection and their expression decreased later at convalescence in the three subsets of monocytes in COVID-19 controls (Figure 4e). In contrast, we did not detect upregulation of these anti-inflammatory genes in COVID-19 CVID patients (Figure 4e).

All these results indicate that upregulation and persistent activation of specific inflammasome genes in the monocytic compartment upon SARS-CoV-2 infection are features of CVID patients. In addition, COVID-19 CVID monocytes show a defective expression of anti-inflammatory genes that might explain the sustained upregulation of inflammasome-related genes observed in COVID-19 CVID patients.

Discussion

Our results show a broad transcriptional dysregulation affecting cell populations of both the innate and the adaptive immunity systems during SARS-CoV-2 infection and subsequent recovery in CVID patients, which give us a unique perspective on the involvement of different immune cells in the response against viral infection in these patients. We observed a dysregulated expression of BCR signaling-related genes and an impaired activation of the canonical NF-κB pathway in naïve B cells of COVID-19 CVID patients. In the NK and T cell compartment, we observed an enhanced cytotoxic activity but impaired cytokine response. Finally we defined a higher and maintained transcriptional activation of inflammasome-related genes in the monocytic compartment of these COVID-19 CVID patients, together with a profound impairment in the transcriptional activation of several anti-inflammatory genes during acute infection (Figure 5).

Remarkably, many of these transcriptional alterations detected in COVID-19 CVID patients were persistent at the convalescence stage. The persistent effects of COVID-19 are a major concern in the context of the current pandemic. In this regard, the defective immunization after COVID-19, the suboptimal response to

anti-SARS-CoV-2 vaccination [45,46] and the observed prolonged viral positivity in some CVID patients, highlight the importance of studying the effect of such suboptimal antibody response on the general immune homeostasis in the context of SARS-CoV-2 infection and subsequent recovery.

It has been reported that type I IFN might have an important role in exacerbating inflammation in the progression to severe COVID-19 [47], although this idea was challenged by another study showing that type I IFN responses are impaired in patients with severe COVID-19 [48]. Our results indicate that type I IFN response is very similar in COVID-19 CVID patients compared with mild COVID-19 controls at the progression stage, but the response is maintained at convalescence in CVID individuals, likely as a consequence of the persistent positivity in these patients.

CVID patients are characterized by displaying hypogammaglobulinemia, profound alterations in the B cell immune response and specially of the memory formation due to an altered germinal centers (GC) function [49,50]. In fact, CVID patients do not respond properly to immunization against SARS-CoV-2 [51], which renders these individuals a potential risk for recurrent and possibly prolonged SARS-CoV-2 infection. In association with the absence of specific antibody response and memory, together with the lack of proper extrafollicular in the early phase and later GC responses in CVID patients, we observed a general increased activation of naïve B cells expressed by the upregulation of BCR signaling-related genes. However, this does not translate into efficient downstream signaling as demonstrated for the impaired NF-κB signal in these cells, a phenomenon observed already in CVID patients, independently of a known acute viral infection [33,52]. This lack of proper NF-κB activation may contribute to the poor GC response, among other factors, by the deficient recruitment of T cells due to reduced NF-κB-dependent CCL3 production [53,54]. Although naïve B cells are not directly involved in the GC reaction, activated naïve B cells in the context of secondary lymphoid organs might constitute a necessary source of this chemokine and other molecules. Our results show that the defective activation of the canonical NF-κB pathway might be caused by the aberrant activity of the NF-κB inhibitor IκBα. In this regard, it has been shown that *in vitro* BCR stimulation of naïve B cells from CVID patients induces an impaired activation of the canonical NF-κB pathway, being this impairment more severe in naïve B cells from CVID patients with higher levels of $CD21^{low}$ B cells and more profound in $CD21^{low}$ B cells [33]. Our data is in line with these previous findings observed *in vitro* and confirm the defective NF-κB activation in CVID B cells upon an *in vivo* immunological challenge caused by SARS-CoV-2 viral infection. This difference in NF-κB activation is not due to an increase of $CD21^{low}$ B cells within the naïve B cell compartment but a cell intrinsic defect of naïve B cells in CVID patients which we were able to ensure through careful gating. As it is impossible that the scarce number of naïve anti-SARS-CoV-2 antigen specific B cells cause the observed general alteration in NF-κB pathway activity, defects in the activation of other receptors upstream to the NF-κB signaling pathway such as toll-like receptors (TLRs) might be involved in the general lower activity of NF-κB observed in naïve B cell of COVID-19 CVID patients. In fact, SARS-CoV-2 ssRNA activates TLR7 and TLR8 [55], and TLR7 has previously been shown to have defective signaling in CVID patients [56].

Our results also show a specific and persistent higher activity of the hypoxia-related TF HIF-1α in naïve B cells from CVID patients upon SARS-CoV-2 infection. In addition to the well described hypoxia-mediated stabilization of HIF-1α, this TF can be induced by hypoxia-independent mechanisms such as BCR/PI3K stimulation [36] or NF-κB activation by toll-like receptors [57]. The fact that these patients showed an impaired NF-κB pathway activation in the naïve B cell compartment, suggests that additional pathways might be involved. Hypoxia has been previously reported to affect B cell function and induce B cell abnormalities in COVID-19 patients [34,35], so this molecular feature might have an additional negative impact on setting up a proper B cell response in these immunodeficient patients.

These alterations of the humoral adaptive immune system in COVID-19 CVID patients occur in the presence of an impaired IFN-γ and TNF-α production in both T cell and NK cell subsets. Similarly to the prolonged positivity observed in our COVID-19 CVID patients, impaired IFN-γ response has been associated with a prolonged course of COVID-19 in immunocompromised individuals [58]. This impaired IFN-γ upregulation would be in line with previously shown defective post-vaccination cellular responses after SARS-CoV-2 vaccination in CVID individuals [46], but still surprising given the TH1 bias that we and others have previously described in CVID patients with $CD21^{low}$ phenotype and immune dysregulation [59]. On the other hand, we observed that both NK and CD8+ T cells from COVID-19 CVID patients strongly upregulate *GZMB* and *PRF1* lytic genes among others, suggesting the existence of a strong cytotoxic response. It remains to be proven whether and how a poor specific antibody response and a reduced cytokine but strong cytotoxic response by T and NK cells relate with the prolonged SARS-CoV2 positivity in these patients.

Altered monocyte activation has been described in CVID patients [18]. Upon SARS-CoV-2 infection, these immunodeficient individuals displayed a dysfunctional and persistent gene upregulation of several components of different inflammasomes complexes, including pyrin (*MEFV*), AIM2 and NLRC4/IPAF inflammasomes in the monocytic compartment. The upregulation of this variety of inflammasomes components would indicate that multiple signals, including both extrinsic virus-related and host-intrinsic mechanisms, may be triggering such transcriptional activation. For instance, NLRP3 inflammasome activation in myeloid cells can be modulated by different SARS-CoV-2 proteins [60,61], and monocytes can be infected by SARS-CoV-2 through anti-spike antibodies-mediated phagocytosis [62], inducing NLRP3 and AIM2 inflammasomes activation. Nevertheless, the defective humoral response that characterizes CVID individuals would discard such possibility, suggesting that the inflammasome hyperactivation observed in COVID-19 CVID patients may be induced by other mechanisms. For instance, different sources of double-stranded DNA (dsDNA) like dead infected cells, damaged mitochondria or bacterial coinfection, a frequent feature in CVID patients, might also result in the presence of cytosolic dsDNA, which would induce the activation of the AIM2 inflammasome [63]. In addition, flagellin derived from *Pseudomonas aeruginosa* or *Salmonella typhimurium*, and bacterial toxins may trigger the activation of the the NLRC4 and pyrin inflammasomes respectively [64,65]. It will be interesting to investigate whether TLR signaling plays a role in the observed alterations and might indicate a relevant contribution of a type of pathogen and related PAMPs.

The inflammatory features observed in the myeloid compartment of COVID-19 CVID patients occur not only during viral infection, but also they are maintained at the convalescent stage. This might be caused by an inefficient viral clearance by the adaptive immune system and a subsequent persistence of viral antigens at different sites. Future studies will determine whether poor viral clearance in immunocompromised patients contributes to the chronic immune activation even in the absence of overt infection as it is observed in CVID.

Identifying the specific immune cell signature alterations in the context of a prototypic infection like SARS-CoV-2, will allow for screening CVID and other immunocompromised patient populations to find similarities and define potential alterations of the immune system even during a supposed convalescence phase.

Inflammation is required for infection clearance, but timely and efficient resolution of the inflammatory response is also crucial to avoid excessive and/or chronic inflammation that might harm the host. In this sense, our results also show that SARS-CoV-2 infection induces upregulation of anti-inflammatory genes such as *IL10*, *ARG1*, *SOCS3* and *PPARG* in the monocytic compartment of COVID-19 controls. Interestingly, these anti-inflammatory genes are not upregulated in COVID-19 CVID patients, which might contribute to the sustained activation of the inflammasome-related genes observed in these immunodeficient patients. Whether this persistent activation might worsen the lung damage present in many CVID patients and, hence, increase the risk of clinical complications, remains to be elucidated in future prospective studies with a larger cohort of patients.

Methods

Study participants and sample collection

Human blood samples were collected from CVID patients as previously diagnosed according to the European society of immune deficiencies (ESID) criteria [66,67] . Samples were collected before (baseline), upon (progression) and after (convalescence) SARS-CoV-2 infection. They were collected at the Medical Center-University of Freiburg, Germany. All donors received oral and written information about the possibility that their blood would be used for research purposes, and any questions that arose were answered. The study was approved by the local Ethics Committees of the participating center (507/16; 282/11). Prior to sample collection, donors signed a consent form approved by the Ethics Committee of their corresponding center, which adhered to the principles set out in the WMA Declaration of Helsinki. PBMCs were obtained from peripheral blood by Ficoll gradient using Lymphocyte Isolation Solution. Once PBMCs had been isolated, all samples were cryopreserved and stored at -150°C.

Single-cell capture

Cryopreserved PBMCs were thawed rapidly in a 37°C water bath, then slowly diluted in pre-warmed growth medium, centrifuged, resuspended in PBS + 0.04% BSA and filtered with a 40 um Bel-art Flowmi strainer. Cells from different donors were counted and concentration adjusted to load 50,000 cells on the

10X-Genomics Chromium Station. In cases where PBMCs from different donors were pooled, a fraction was taken to isolate genomic DNA for genotyping, using Illumina Infinium Global Screening Array, and the other fraction was used to generate single-cell gel beads-in-emulsion (GEMs). Genomic DNA was isolated from PBMCs for genotyping using a Maxwell® 16 Blood DNA Purification Kit from Promega following the manufacturer's instructions.

Library generation and sequencing

Libraries were constructed following the manufacturer's protocol for the Chromium Next GEM Single Cell V(D)J Reagent Kits v1.1 with Feature Barcode technology for Cell Surface Protein (10X Genomics Rev E), but with two amendments: the amount of SI primer was doubled, and the number of PCR cycles was set at 7. Samples were sequenced using the Illumina NovaSeq 6000, where cellular gene expression, as well as B cell and T cell clonality were simultaneously profiled. We targeted ~300M raw reads per sample (~60,000 raw reads per cell) with cycle numbers of 100 for read 1, 100 for read 2, and 100 for the index read.

Single-cell data alignment, quantification, and quality control

The single-cell transcriptome data were aligned and quantified by Cell Ranger v3.1 using GRCh38 (Ensembl 93) concatenated to the SARS-Cov-2 genome as a reference. Pooled donor samples were deconvolved using Souporcell [68], which yielded a genotype variant that allowed donor identity to be matched across samples. Cells that could not be explained by a single genotype were considered doublets and removed before analysis. Additionally, Scrublet [69] was employed to detect and remove other doublets by computing a doublet score for each cell, evaluated independently in each sample. Doublets filtered in the downstream analysis are defined by a Student's *t*-test ($p < 0.01$) with Bonferroni correction, which was used for each cell's score compared to that score distribution found within fine-grained sub-clustering of each cluster produced by the Leiden algorithm . Furthermore, genes expressed in fewer than three cells, and cells with fewer than 200 genes or more than 20% mitochondrial gene content were removed.

Deconvolution of donors in pooled scRNA-seq samples

Pooled scRNA-seq samples containing cells from multiple individuals were demultiplexed using souporcell. Briefly, the algorithm identifies genotypic differences between single cells by variant calling aligned reads using STAR [70] and generating a VCF (Variant Call Format) file using Freebayes (Marth 2012). Souporcell was run with the following command for all samples (argument $1 corresponds to sample ID, and N is the number of multiplexed individuals in a sample): /software/singularity-v3.5.1/bin/singularity exec./souporcell.sif./souporcell_pipeline.py -i./cellranger302_count_$1_GRCh38-1_2_0/possorted_genome_bam.bam -b./cellranger302_count_$1_GRCh38-1_2_0/filtered_feature_bc_matrix/barcodes.tsv -f./refdata-cellranger-GRCh38-1.2.0/fasta/genome.fa -t 8 -o souporcell_result_$1 -k N --skip_remap True --common_variants./filtered_2p_1kgenomes_GRCh38.vcf, where the last VCF file with common variants was downloaded as per instructions in

https://github.com/wheaton5/souporcell with the following command: wget –load-cookies /tmp/cookies.txt “https://docs.google.com/uc?export=download&confirm=$(wget-quiet-save-cookies/tmp/cookies.txt-keep-session-cookies-no-check-certificate ‘ https ://docs.google.com/uc?export=download&id=13aebUpEKrtjliyT9rYzRijtkNJVUk5F_’-O-|sed-rn’s/. *confirm=([0-9A-Za-z_]+).*/\1\n/p’)&id=13aebUpEKrtjliyT9rYzRijtkNJVUk5F_”-Ocommon_variants_grch38.vcf && rm-rf/tmp/cookies.txt.

Furthermore, to find out the exact donor identity of each donor’s barcode cluster in souporcell results, the cells in parallel have undergone genotyping using Illumina Infinium Global Screening Array. In order to unambiguously identify every individual in the pooled samples, each donor’s variants were separated from the pooled VCF and each single-donor VCF was matched to the genotype data using PLINK [71]. This software matches each souporcell sample with the genotype data giving a concordance ratio (based on the similarity of the variants) that allows us to distinctly identify each sample with each donor ID.

Cell type identification and cluster annotation

Scvi was used to integrate single cells from external datasets in order to identify comparable cell types for subsequent different gene expression analysis. Generative models with 64 latent variables were used to model the 5000 variable gene detected in the combined datasets. Manifolds that overlay T cell, B cell or monocyte compartments were obtained by modeling each subset with only 20 latent variables instead. Louvain clustering and umap were similarly obtained using the Scanpy toolkit [72]. Preliminary annotations were defined using the external datasets identified cell types, and manual refinement using the expression of known cell-specific marker genes was used whenever such annotations showed limited agreement in the unsupervised clusters obtained from the Louvain algorithm. In addition, the annotation performed was validated using the tool Azimuth [73].

T cell receptor and B cell receptor clonality

Single-cell TCR data were processed with the Cell Ranger v3.1 vdj pipeline using GRCh38 as a reference. Downstream analysis was then performed using Scirpy [74]. In particular, only cells with at least one α-chain and one β-chain but fewer than two full pairs of α/β chains were kept for analysis, and expanded clones were defined when a clonotype was present in more than one cell. Many clonotypes were detected at several stages of the progression of the disease; we could define three categories corresponding to the earliest time point where the clone was detected as expanded in the baseline, progression and convalescence samples. The BCR data was similarly processed by cellranger v3.1 vdj pipeline, and the prevalence of IGHV genes was compared directly to what was reported by the study of the control cohort without primary immunodeficiency [27].

Differential gene expression

Comparison of gene expression was performed either between our cohort of CVID patients and with corresponding control cohorts from [27], or alternatively between timepoints within the CVID or non-CVID

cohort. Both wilcoxon test and deseq2 [75] were used to identify differentially expressed genes. For the wilcoxon test, the two sets of cells whose expression is to be compared are each partitioned into 4 groups based on the quartile for their total UMI count, so that wilcoxon tests would be performed on each matching quartile. For each quartile, the group of cells with the higher UMI count per cell would have its counts randomly downsampled to better match the other; then, the resulting 4 z-scores are combined. Instead of controlling for sequencing depth, we use DESEQ2 to account for patient specific variability by forming mini-bulk samples for each individual considered.

Type I interferon, citotoxicity and anti-inflammatory scores calculation

For interferon score calculation, a list of genes related to type I IFN response was obtained from the GSEA molecular Signatures Database (GO:0034340). For cytotoxicity score calculation, a list of cytotoxic-related genes was selected, including *GZMA*, *GZMB*, *GZMH*, *GZMK*, *GZMM*, *PRF1*, *NKG7*, *GNLY*, *NRC3*, *FGFBP2* and *KLRD1*. For anti-inflammatory score calculation, a list of anti-inflammatory genes was selected, including *IL10*, *PPARG*, *SOCS3*, *ARG1*, *CTSD*, *CD63*, *MMP9* and *ADM*. Scores were calculated in each cell type and in each SARS-CoV-2 infection stage (baseline, progression or convalescence) subtracting the average expression of all genes from the average expression of the genes in each list. Then, score enrichments were calculated for progression or convalescence over baseline.

Gene ontology analysis

Based on the DEGs for progression and convalescence over baseline in each cell subtype, GO terms enrichment was obtained using the R package clusterProfiler [76] with the default parameters. Annotation Dbi R package “org.Hs.eg.db” was used to map gene identifiers.

Transcription factor activity analysis

Inference of TF activities from expression values were calculated using DoRothEA [77], a curated resource of TFs and their targets compiled from various sources including the literature, ChIP-Seq peaks, *in silico* predictions, as well as gene expression data, was used to estimate TF activities from combined expression values of gene targets. The A_viperRegulon.rdata dataset was loaded in R and its Integrated Development Environment (RStudio) and used for the analysis.

Statistical analysis

Statistical analyses were performed in R (v4.0.3). Differences in the representation of cell types was reported using two-tailed Welch's t tests, comparing the proportion of cell types in each patient between the CVID and non-CVID cohorts.

Declarations

ACKNOWLEDGEMENTS

We thank the CERCA Program/Generalitat de Catalunya and the Josep Carreras Foundation for institutional support. This publication is part of the Human Cell Atlas: www.humancellatlas.org/publications. This study was funded by ”la Caixa” Foundation under the grant agreement LCF/PR/HR22/52420002, Spanish Ministry of

Science and Innovation (grant number PID2020-117212RB-I00/AEI/10.13038/501100011033) (E.B.), by the Wellcome Trust Grant 206194 and 108413/A/15/D (R.V.-T.), Instituto de Salud Carlos III (ISCIII), Ref. AC18/00057, associated with i-PAD project (ERARE European Union program) (E.B.), and the Chan Zuckerberg Initiative (grant 2020-216799) (R.V.-T. and E.B.). This publication has also been supported by the Unstoppable campaign of the Josep Carreras Leukaemia Foundation. We are indebted to the donors for participating in this research.

AUTHOR CONTRIBUTIONS

J.R.-U., K.W., R.V.-T. and E.B. conceived the study; J.R.-U., L.C. and G.G.-T. performed 10X Chromium experiments; J.R.-U., G.G.-T., R.H., T.P. and E.P. performed sample and library preparation; E.A.-L. and J.M. performed patient genotyping; J.R-U., L.-F. H., C.C.-F. and J.C.-S. performed computational analysis; J.R.-U., L.-F. H., B.K., C.C.-F., G.G.-T., J.C.-S., K.W., R.V.-T. and E.B. analyzed and interpreted the data; B.K., M.H., A.D. and K.W. contributed with clinical material and clinical interpretation of the results; J.R-U. and E.B. wrote the manuscript with contributions from L.-F. H., B.K, K.W. and R.V-T.; K.W., R.V.-T. and E.B. co-directed the study. All authors read and accepted the paper.

DATA ACCESS

Chromium droplet-based scRNA-seq data can be accessed under EGA dataset accession. Interactive visualizations of single-cell transcriptomic datasets from this study can be accessed via https://www.immunodeficiencycellatlas.org/comparison (username: cvid; password: cvid@2022).

CONFLICTS OF INTEREST

The authors declare no competing interests.

References

1. Gavriatopoulou, M. *et al.* Organ-specific manifestations of COVID-19 infection. *Clin. Exp. Med.* **20**, 493–506 (2020).
2. Mehandru, S. & Merad, M. Pathological sequelae of long-haul COVID. *Nat. Immunol.* **23**, 194–202 (2022).
3. Tan, A. T. *et al.* Early induction of functional SARS-CoV-2-specific T cells associates with rapid viral clearance and mild disease in COVID-19 patients. *Cell Rep.* **34**, 108728 (2021).
4. Braun, J. *et al.* SARS-CoV-2-reactive T cells in healthy donors and patients with COVID-19. *Nature* **587**, 270–274 (2020).

5. Rydyznski Moderbacher, C. *et al.* Antigen-Specific Adaptive Immunity to SARS-CoV-2 in Acute COVID-19 and Associations with Age and Disease Severity. *Cell* **183**, 996-1012.e19 (2020).
6. Peng, Y. *et al.* Broad and strong memory CD4+ and CD8+ T cells induced by SARS-CoV-2 in UK convalescent individuals following COVID-19. *Nat. Immunol.* **21**, 1336–1345 (2020).
7. Hartley, G. E. *et al.* Rapid generation of durable B cell memory to SARS-CoV-2 spike and nucleocapsid proteins in COVID-19 and convalescence. *Sci. Immunol.* **5**, (2020).
8. Gaebler, C. *et al.* Evolution of antibody immunity to SARS-CoV-2. *Nature* **591**, 639–644 (2021).
9. Robbiani, D. F. *et al.* Convergent antibody responses to SARS-CoV-2 in convalescent individuals. *Nature* **584**, 437–442 (2020).
10. Schulte-Schrepping, J. *et al.* Severe COVID-19 Is Marked by a Dysregulated Myeloid Cell Compartment. *Cell* **182**, 1419-1440.e23 (2020).
11. Schultze, J. L. & Aschenbrenner, A. C. COVID-19 and the human innate immune system. *Cell* **184**, 1671–1692 (2021).
12. Sette, A. & Crotty, S. Adaptive immunity to SARS-CoV-2 and COVID-19. *Cell* **184**, 861–880 (2021).
13. Seidel, M. G. *et al.* The European Society for Immunodeficiencies (ESID) Registry Working Definitions for the Clinical Diagnosis of Inborn Errors of Immunity. *J. allergy Clin. Immunol. Pract.* **7**, 1763–1770 (2019).
14. Bonilla, F. A. *et al.* International Consensus Document (ICON): Common Variable Immunodeficiency Disorders. *J. allergy Clin. Immunol. Pract.* **4**, 38–59 (2016).
15. Ameratunga, R. Assessing Disease Severity in Common Variable Immunodeficiency Disorders (CVID) and CVID-Like Disorders. *Front. Immunol.* **9**, 2130 (2018).
16. Bateman, E. A. L. *et al.* T cell phenotypes in patients with common variable immunodeficiency disorders: associations with clinical phenotypes in comparison with other groups with recurrent infections. *Clin. Exp. Immunol.* **170**, 202–11 (2012).
17. Azizi, G. *et al.* Circulating Helper T-Cell Subsets and Regulatory T Cells in Patients With Common Variable Immunodeficiency Without Known Monogenic Disease. *J. Investig. Allergol. Clin. Immunol.* **28**, 172–181 (2018).
18. Barbosa, R. R. *et al.* Monocyte activation is a feature of common variable immunodeficiency irrespective of plasma lipopolysaccharide levels. *Clin. Exp. Immunol.* **169**, 263–72 (2012).
19. Cambronero, R., Sewell, W. A., North, M. E., Webster, A. D. & Farrant, J. Up-regulation of IL-12 in monocytes: a fundamental defect in common variable immunodeficiency. *J. Immunol.* **164**, 488–94 (2000).
20. Marcus, N. *et al.* Minor Clinical Impact of COVID-19 Pandemic on Patients With Primary Immunodeficiency in Israel. *Front. Immunol.* **11**, 614086 (2021).
21. Drabe, C. H. *et al.* Low morbidity in Danish patients with common variable immunodeficiency disorder infected with severe acute respiratory syndrome coronavirus 2. *Infect. Dis. (London, England)* **53**, 953–958 (2021).

22. Cohen, B. *et al.* COVID-19 infection in 10 common variable immunodeficiency patients in New York City. *J. allergy Clin. Immunol. Pract.* **9**, 504-507.e1 (2021).
23. Milito, C. *et al.* Clinical outcome, incidence, and SARS-CoV-2 infection-fatality rates in Italian patients with inborn errors of immunity. *J. allergy Clin. Immunol. Pract.* **9**, 2904-2906.e2 (2021).
24. Shields, A. M., Burns, S. O., Savic, S., Richter, A. G. & UK PIN COVID-19 Consortium. COVID-19 in patients with primary and secondary immunodeficiency: The United Kingdom experience. *J. Allergy Clin. Immunol.* **147**, 870-875.e1 (2021).
25. Milito, C., Soccodato, V., Auria, S., Pulvirenti, F. & Quinti, I. COVID-19 in complex common variable immunodeficiency patients affected by lung diseases. *Curr. Opin. Allergy Clin. Immunol.* **21**, 535–544 (2021).
26. Katzenstein, T. L. *et al.* Outcome of SARS-CoV-2 infection among patients with common variable immunodeficiency and a matched control group: A Danish nationwide cohort study. *Front. Immunol.* **13**, 994253 (2022).
27. Ren, X. *et al.* COVID-19 immune features revealed by a large-scale single-cell transcriptome atlas. *Cell* **184**, 1895-1913.e19 (2021).
28. Stephenson, E. *et al.* Single-cell multi-omics analysis of the immune response in COVID-19. *Nat. Med.* **27**, 904–916 (2021).
29. McNab, F., Mayer-Barber, K., Sher, A., Wack, A. & O'Garra, A. Type I interferons in infectious disease. *Nat. Rev. Immunol.* **15**, 87–103 (2015).
30. Lee, J. S. & Shin, E.-C. The type I interferon response in COVID-19: implications for treatment. *Nat. Rev. Immunol.* **20**, 585–586 (2020).
31. Galbraith, M. D. *et al.* Specialized interferon action in COVID-19. *Proc. Natl. Acad. Sci. U. S. A.* **119**, (2022).
32. Wehr, C. *et al.* The EUROclass trial: defining subgroups in common variable immunodeficiency. *Blood* **111**, 77–85 (2008).
33. Keller, B. *et al.* Disturbed canonical nuclear factor of κ light chain signaling in B cells of patients with common variable immunodeficiency. *J. Allergy Clin. Immunol.* **139**, 220-231.e8 (2017).
34. Burrows, N. *et al.* Dynamic regulation of hypoxia-inducible factor-1α activity is essential for normal B cell development. *Nat. Immunol.* **21**, 1408–1420 (2020).
35. Kotagiri, P. *et al.* The impact of hypoxia on B cells in COVID-19. *EBioMedicine* **77**, 103878 (2022).
36. Harder, I. *et al.* Dysregulated PI3K Signaling in B Cells of CVID Patients. *Cells* **11**, (2022).
37. Yuan, M. *et al.* Structural basis of a shared antibody response to SARS-CoV-2. *Science* **369**, 1119–1123 (2020).
38. Cao, Y. *et al.* Potent Neutralizing Antibodies against SARS-CoV-2 Identified by High-Throughput Single-Cell Sequencing of Convalescent Patients' B Cells. *Cell* **182**, 73-84.e16 (2020).
39. Kuri-Cervantes, L. *et al.* Comprehensive mapping of immune perturbations associated with severe COVID-19. *Sci. Immunol.* **5**, (2020).

40. Sattler, A. *et al.* SARS-CoV-2-specific T cell responses and correlations with COVID-19 patient predisposition. *J. Clin. Invest.* **130**, 6477–6489 (2020).
41. Maucourant, C. *et al.* Natural killer cell immunotypes related to COVID-19 disease severity. *Sci. Immunol.* **5**, (2020).
42. Kvedaraite, E. *et al.* Major alterations in the mononuclear phagocyte landscape associated with COVID-19 severity. *Proc. Natl. Acad. Sci. U. S. A.* **118**, (2021).
43. Vanderbeke, L. *et al.* Monocyte-driven atypical cytokine storm and aberrant neutrophil activation as key mediators of COVID-19 disease severity. *Nat. Commun.* **12**, 4117 (2021).
44. Brauns, E. *et al.* Functional reprogramming of monocytes in patients with acute and convalescent severe COVID-19. *JCI insight* **7**, (2022).
45. Fernandez Salinas, A. *et al.* Impaired memory B-cell response to the Pfizer-BioNTech COVID-19 vaccine in patients with common variable immunodeficiency. *J. Allergy Clin. Immunol.* **149**, 76–77 (2022).
46. Arroyo-Sánchez, D. *et al.* Immunogenicity of Anti-SARS-CoV-2 Vaccines in Common Variable Immunodeficiency. *J. Clin. Immunol.* **42**, 240–252 (2022).
47. Lee, J. S. *et al.* Immunophenotyping of COVID-19 and influenza highlights the role of type I interferons in development of severe COVID-19. *Sci. Immunol.* **5**, (2020).
48. Hadjadj, J. *et al.* Impaired type I interferon activity and inflammatory responses in severe COVID-19 patients. *Science* **369**, 718–724 (2020).
49. Romberg, N. *et al.* Patients with common variable immunodeficiency with autoimmune cytopenias exhibit hyperplastic yet inefficient germinal center responses. *J. Allergy Clin. Immunol.* **143**, 258–265 (2019).
50. Unger, S. *et al.* Ill-defined germinal centers and severely reduced plasma cells are histological hallmarks of lymphadenopathy in patients with common variable immunodeficiency. *J. Clin. Immunol.* **34**, 615–26 (2014).
51. Bergman, P. *et al.* Elevated CD21low B Cell Frequency Is a Marker of Poor Immunity to Pfizer-BioNTech BNT162b2 mRNA Vaccine Against SARS-CoV-2 in Patients with Common Variable Immunodeficiency. *J. Clin. Immunol.* **42**, 716–727 (2022).
52. Freudenhammer, M., Voll, R. E., Binder, S. C., Keller, B. & Warnatz, K. Naive- and Memory-like CD21low B Cell Subsets Share Core Phenotypic and Signaling Characteristics in Systemic Autoimmune Disorders. *J. Immunol.* **205**, 2016–2025 (2020).
53. Castellino, F. *et al.* Chemokines enhance immunity by guiding naive CD8+ T cells to sites of CD4+ T cell-dendritic cell interaction. *Nature* **440**, 890–5 (2006).
54. Benet, Z. L. *et al.* CCL3 Promotes Germinal Center B Cells Sampling by Follicular Regulatory T Cells in Murine Lymph Nodes. *Front. Immunol.* **9**, 2044 (2018).
55. Salvi, V. *et al.* SARS-CoV-2-associated ssRNAs activate inflammation and immunity via TLR7/8. *JCI insight* **6**, (2021).

56. Yu, J. E. *et al.* Toll-like receptor 7 and 9 defects in common variable immunodeficiency. *J. Allergy Clin. Immunol.* **124**, 349–56, 356.e1–3 (2009).
57. Blouin, C. C., Pagé, E. L., Soucy, G. M. & Richard, D. E. Hypoxic gene activation by lipopolysaccharide in macrophages: implication of hypoxia-inducible factor 1alpha. *Blood* **103**, 1124–30 (2004).
58. van Laarhoven, A. *et al.* Interferon gamma immunotherapy in five critically ill COVID-19 patients with impaired cellular immunity: A case series. *Med (New York, N.Y.)* **2**, 1163-1170.e2 (2021).
59. Unger, S. *et al.* The TH1 phenotype of follicular helper T cells indicates an IFN-γ-associated immune dysregulation in patients with CD21low common variable immunodeficiency. *J. Allergy Clin. Immunol.* **141**, 730–740 (2018).
60. Pan, P. *et al.* SARS-CoV-2 N protein promotes NLRP3 inflammasome activation to induce hyperinflammation. *Nat. Commun.* **12**, 4664 (2021).
61. Yalcinkaya, M. *et al.* Modulation of the NLRP3 inflammasome by Sars-CoV-2 Envelope protein. *Sci. Rep.* **11**, 24432 (2021).
62. Junqueira, C. *et al.* FcγR-mediated SARS-CoV-2 infection of monocytes activates inflammation. *Nature* **606**, 576–584 (2022).
63. Vora, S. M., Lieberman, J. & Wu, H. Inflammasome activation at the crux of severe COVID-19. *Nat. Rev. Immunol.* **21**, 694–703 (2021).
64. Wen, J. *et al.* Updating the NLRC4 Inflammasome: from Bacterial Infections to Autoimmunity and Cancer. *Front. Immunol.* **12**, 702527 (2021).
65. Schnappauf, O., Chae, J. J., Kastner, D. L. & Aksentijevich, I. The Pyrin Inflammasome in Health and Disease. *Front. Immunol.* **10**, 1745 (2019).
66. Bousfiha, A. *et al.* The 2017 IUIS Phenotypic Classification for Primary Immunodeficiencies. *J. Clin. Immunol.* **38**, 129–143 (2018).
67. Ameratunga, R. *et al.* Comparison of diagnostic criteria for common variable immunodeficiency disorder. *Front. Immunol.* **5**, 415 (2014).
68. Heaton, H. *et al.* Souporcell: robust clustering of single-cell RNA-seq data by genotype without reference genotypes. *Nat. Methods* **17**, 615–620 (2020).
69. Wolock, S. L., Lopez, R. & Klein, A. M. Scrublet: Computational Identification of Cell Doublets in Single-Cell Transcriptomic Data. *Cell Syst.* **8**, 281-291.e9 (2019).
70. Dobin, A. *et al.* STAR: ultrafast universal RNA-seq aligner. *Bioinformatics* **29**, 15–21 (2013).
71. Purcell, S. *et al.* PLINK: a tool set for whole-genome association and population-based linkage analyses. *Am. J. Hum. Genet.* **81**, 559–75 (2007).
72. Wolf, F. A., Angerer, P. & Theis, F. J. SCANPY: large-scale single-cell gene expression data analysis. *Genome Biol.* **19**, 15 (2018).
73. Hao, Y. *et al.* Integrated analysis of multimodal single-cell data. *Cell* **184**, 3573-3587.e29 (2021).
74. Sturm, G. *et al.* Scirpy: a Scanpy extension for analyzing single-cell T-cell receptor-sequencing data. *Bioinformatics* **36**, 4817–4818 (2020).

75. Love, M. I., Huber, W. & Anders, S. Moderated estimation of fold change and dispersion for RNA-seq data with DESeq2. *Genome Biol.* **15**, 550 (2014).
76. Yu, G., Wang, L.-G., Han, Y. & He, Q.-Y. clusterProfiler: an R package for comparing biological themes among gene clusters. *OMICS* **16**, 284–7 (2012).
77. Garcia-Alonso, L., Holland, C. H., Ibrahim, M. M., Turei, D. & Saez-Rodriguez, J. Benchmark and integration of resources for the estimation of human transcription factor activities. *Genome Res.* **29**, 1363–1375 (2019).

Figures

Figure 1

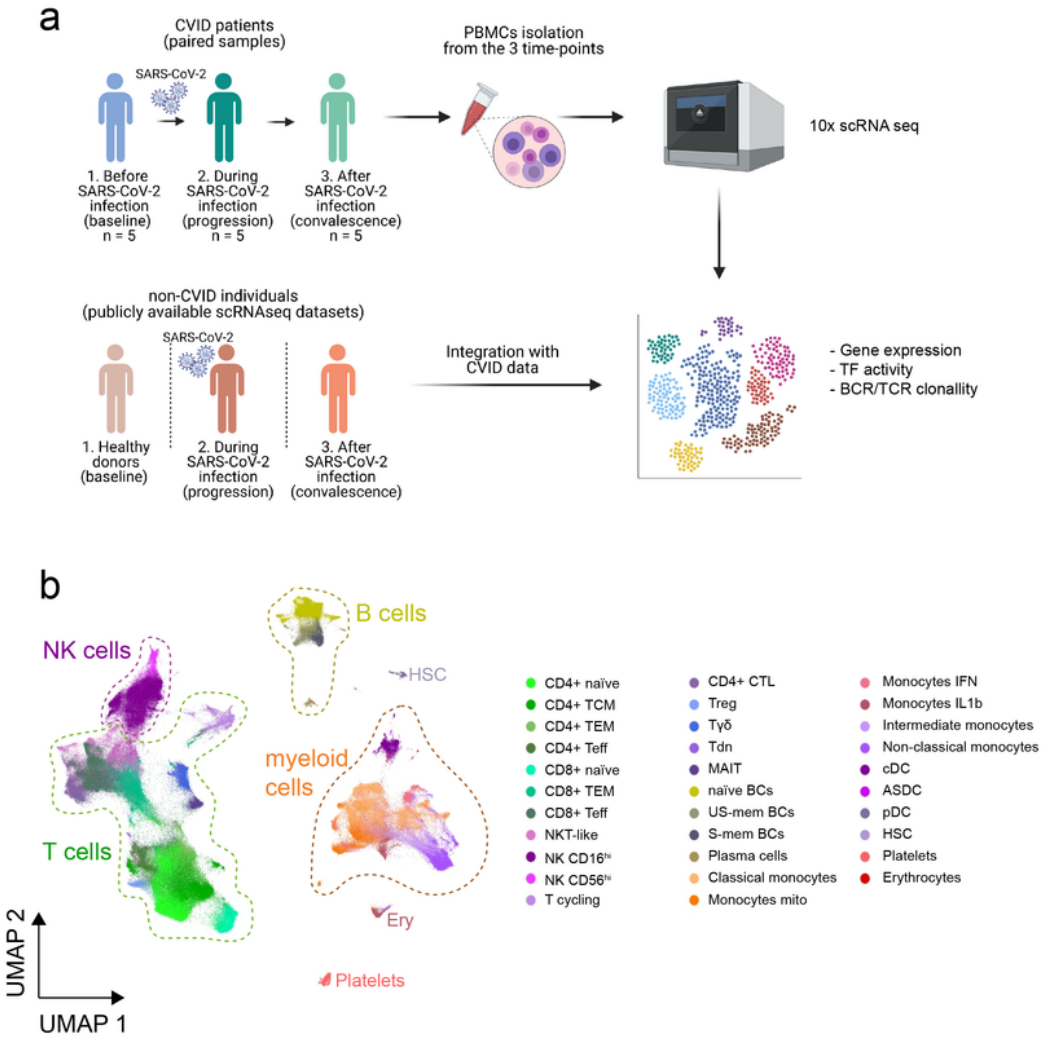

Figure 1

Multi-stage single-cell analysis of PBMCs from COVID-19 patients and controls with or without CVID. (a) Overview of the participants included in the study, the samples collected and the data generated. Panel was created using BioRender.com. (b) UMAP visualization showing different immune cell populations identified from Leiden clustering and cell-specific marker gene expression. The B cell compartment is outlined with a yellow dotted line and includes naïve B cells, un-switched memory B cells, switched

memory B cells, CD21^{low} B cells and plasma cells (PCs). The T cell compartment is outlined with a green dotted line and includes naïve CD4$^+$ T cells, effector memory CD4$^+$ T (CD4$^+$ T_{EM}) cells, central memory CD4$^+$ T (CD4$^+$ T_{CM}) cells, effector CD4$^+$ T cells (CD4$^+$ T_{Eff}), regulatory T (T_{reg}) cells, cytotoxic CD4$^+$ T (CD4$^+$ CTL) cells, naïve CD8$^+$ T cells, effector memory CD8$^+$ T (CD8$^+$ T_{EM}) cells, effector CD8$^+$ T (CD8$^+$ T_{Eff}) cells, mucosal-associated invariant T (MAIT) cells, gamma-delta T ($T_{\gamma\delta}$) cells, double negative T (T_{DN}) cells, cycling T ($T_{cycling}$) cells and NKT-like (NKT) cells. The NK cell compartment is outlined with a purple dotted line and includes NK CD16^{high} and NK CD56^{high} cells. Myeloid cell compartment is outlined with an orange dotted line and includes classical, intermediate and non-classical monocytes, as well as conventional dendritic cells (cDC) and plasmacytoid dendritic cells (pDCs). Three additional clusters of monocytes were annotated as monocytes_IFN, monocytes_IL1b and monocytes_mit. In addition we captured hematopoietic stem cells (HSC) and platelets. (c) Circle plot showing type I IFN response score. Circle size indicates the TPM mean of the list of genes included into the gene ontology category GO:0034340 in each cell type and condition. Scale indicates the fold change of the scores calculated in progression or convalescence over baseline.

Figure 2

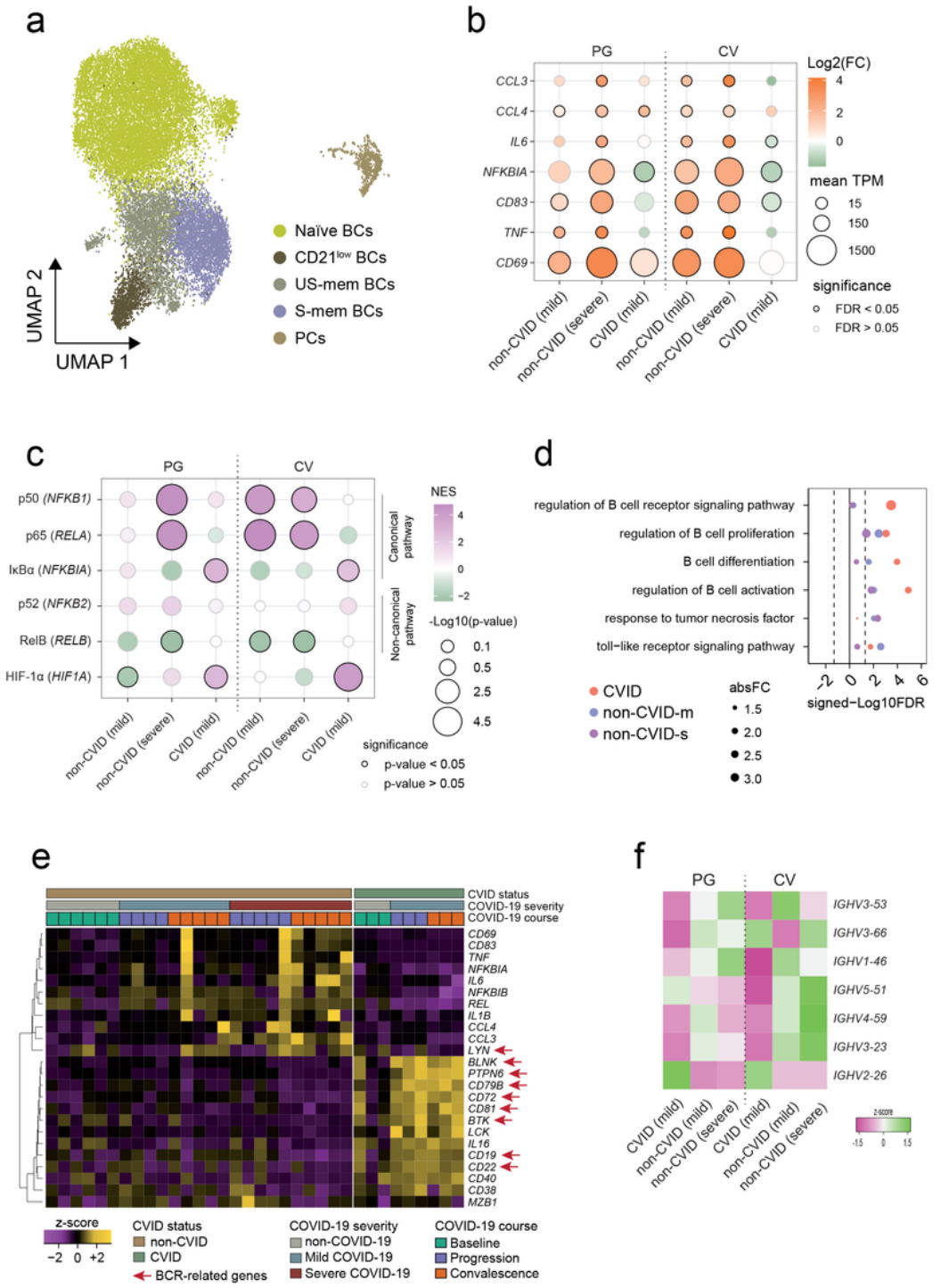

Figure 2

Dysfunctional long-term B cell NF-κB pathway response to SARS-CoV-2 in CVID. (a) UMAP visualization showing different B cell subpopulations identified from Leiden clustering and cell-specific marker gene expression. (b) Circle plot showing the expression of selected genes regulated by the canonical NF-κB pathway. Circle size indicates TPM mean, scale indicates Log2 of gene expression fold change in progression or convalescence over baseline. Significance is also indicated by a black (FDR < 0.05) or gray

(FDR > 0.05) line. (c) Circle plot indicating the transcription factor activity of members of the canonical and non-canonical NF-κB pathways, as well as HIF-1α. Scale indicates the normalized enrichment score (NES) and circle size represents the -Log10 of p-value. Significance is also indicated by a black (p-value < 0.05) or gray (p-value > 0.05) line. (d) Dot plot representing the relative enrichment of naïve B cells from COVID-19 non-CVID and COVID-19 CVID in selected GO categories. Dot size indicates the absolute FC. The DEGs used were those from the comparison between baseline and progression. (e) Heatmap showing the relative expression of selected dysregulated genes in CVID patients compared with healthy controls during SARS-CoV-2 infection. Scale indicates relative gene expression (z-score). Relative gene expression is normalized with respect to the baseline of each dataset (control or CVID). COVID-19 course (baseline, progression or convalescence), COVID-19 severity (mild or severe) and CVID status (CVID or non-CVID) are indicated. In addition, BCR-related genes are indicated with a red arrow. (f) Heatmap representing the relative expression of selected IGHV genes associated with SARS-CoV-2 spike neutralizing antibodies in naïve B cells from COVID-19 non-CVID and COVID-19 CVID patients at progression and convalescence stages. Scale indicates relative gene expression (z-score).

Figure 3

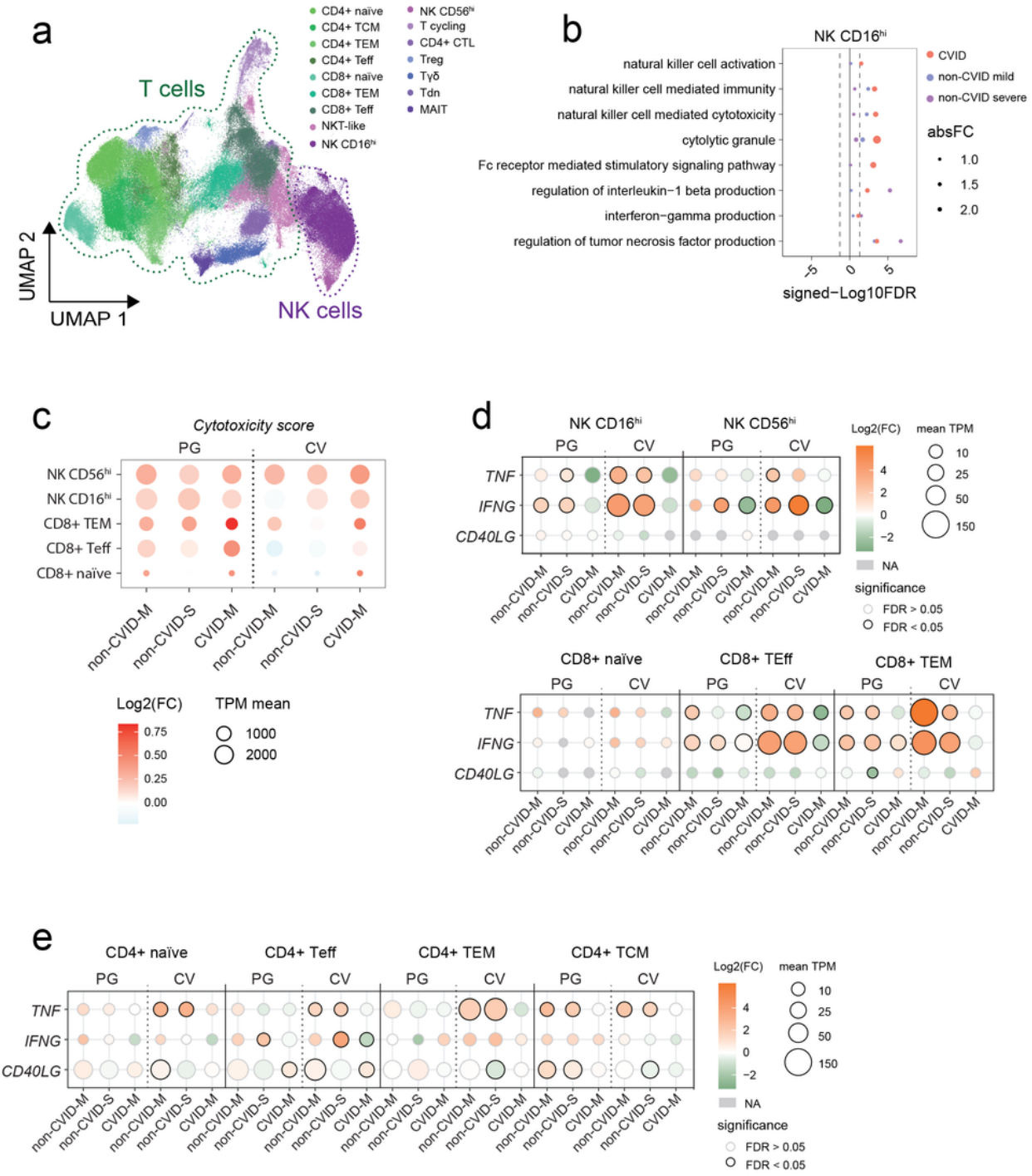

Figure 3

Incomplete NK and T cell responses in COVID-19 CVID patients. (a) UMAP visualization showing different NK and T cell subpopulations identified from Leiden clustering and cell-specific marker gene expression. (b) Circle plot representing the enrichment of several GO categories in CD16^{bright} NK cells at the progression stage compared with baseline. X-axis indicates the signed -Log10 of FDR (positive if the category is enriched and negative if the category is depleted), whereas circle size indicates the absolute

enrichment fold change value. (c) Circle plot representing the relative expression score of selected cytotoxic-related genes in NK y CD8+ T cells. Circle size indicates TPM mean and scale indicates Log2 of the expression score fold change in progression or convalescence states over baseline. PG (progression), CV (convalescence), M (mild), S (severe). (d) Circle plot showing the expression fold change of *IFNG* and *TNF* genes in selected cytotoxic cell subsets. Circle size indicates TPM mean and scale indicates Log2 of the gene expression fold change in progression or convalescence states over baseline. Gray color is indicated for NA values. Significance is also indicated by a black (FDR < 0.05) or gray (FDR > 0.05) line. (e) Circle plot showing the expression fold change of *IFNG*, *TNF* and *CD40LG* genes in selected CD4+ T cell subsets. Circle size indicates TPM mean and scale indicates Log2 of the gene expression fold change in progression or convalescence states over baseline. Gray color is indicated for NA values. Significance is also indicated by a black (FDR < 0.05) or gray (FDR > 0.05) line.

Figure 4

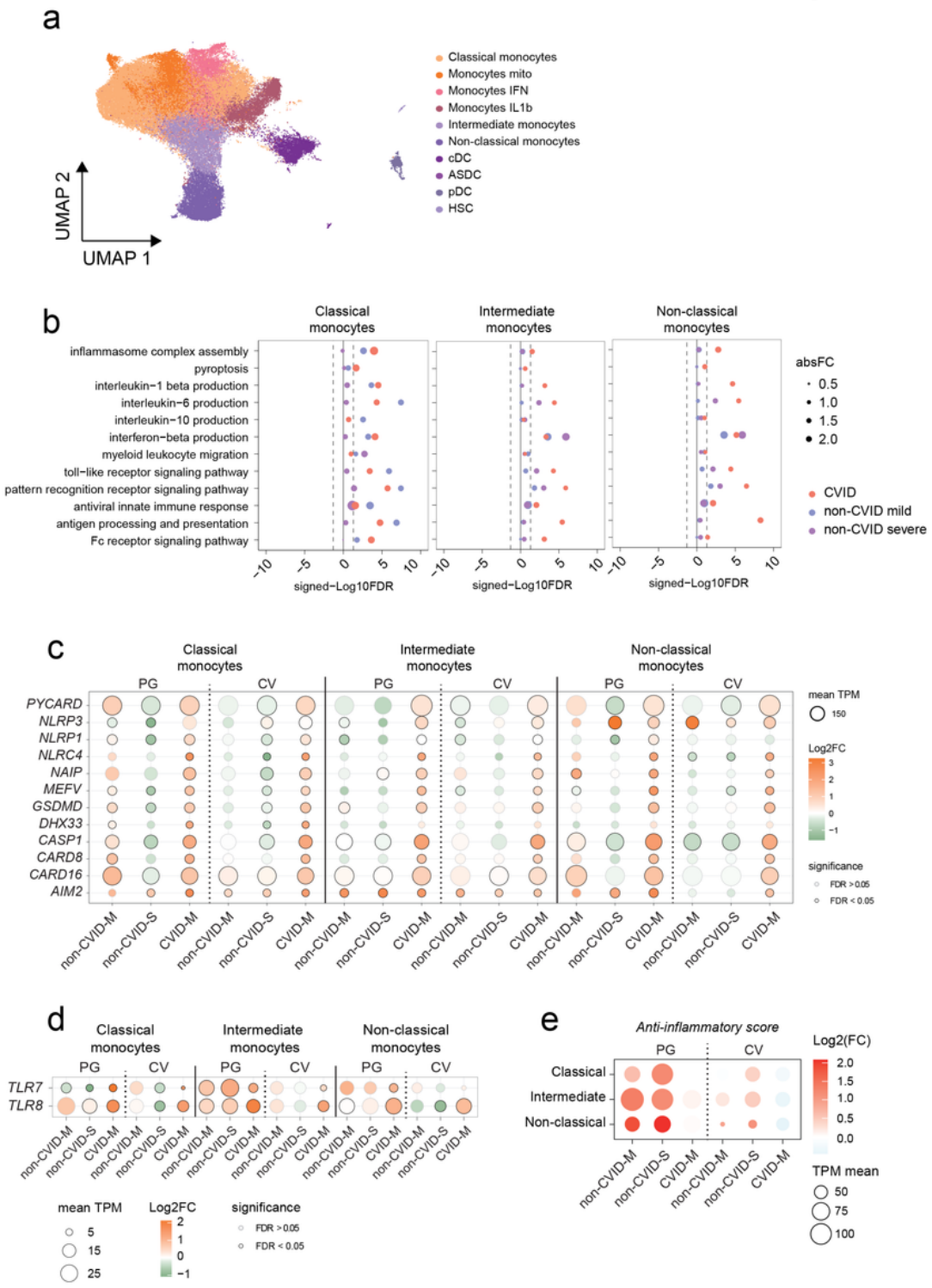

Figure 4

Persistent inflammasome activation and altered chemokine response in monocytes from COVID-19 CVID patients. (a) UMAP visualization of the myeloid compartment showing different myeloid cell populations identified from Leiden clustering and cell-specific marker gene expression. (b) Circle plot showing the enrichment of selected GO in the three main subsets of monocytes, using differentially expressed genes obtained from progression over baseline comparison. Circle size indicates absolute enrichment FC. Color

indicates the three conditions (COVID-19 CVID patients in red, mild COVID-19 controls in blue and severe COVID-19 controls in purple). (c) Circle plot representing the relative expression of selected inflammasome-related genes in the three main monocyte subsets. Circle size indicates TPM mean and scale indicates Log2 of the gene expression fold change in progression or convalescence states over baseline. Significance is also indicated by a black (FDR < 0.05) or gray (FDR > 0.05) line. PG (progression), CV (convalescence), M (mild), S (severe). (d) Circle plot representing the relative expression of *TLR7* and *TLR8* genes in the three main monocyte subsets. Circle size indicates TPM mean and scale indicates Log2 of the gene expression fold change in progression or convalescence states over baseline. Significance is also indicated by a black (FDR < 0.05) or gray (FDR > 0.05) line. PG (progression), CV (convalescence), M (mild), S (severe). (e) Circle plot representing the relative expression score of several anti-inflammatory genes in the three main monocyte subsets. Circle size indicates TPM mean and scale indicates Log2 of the expression score fold change in progression or convalescence states over baseline. PG (progression), CV (convalescence), M (mild), S (severe).

Figure 5

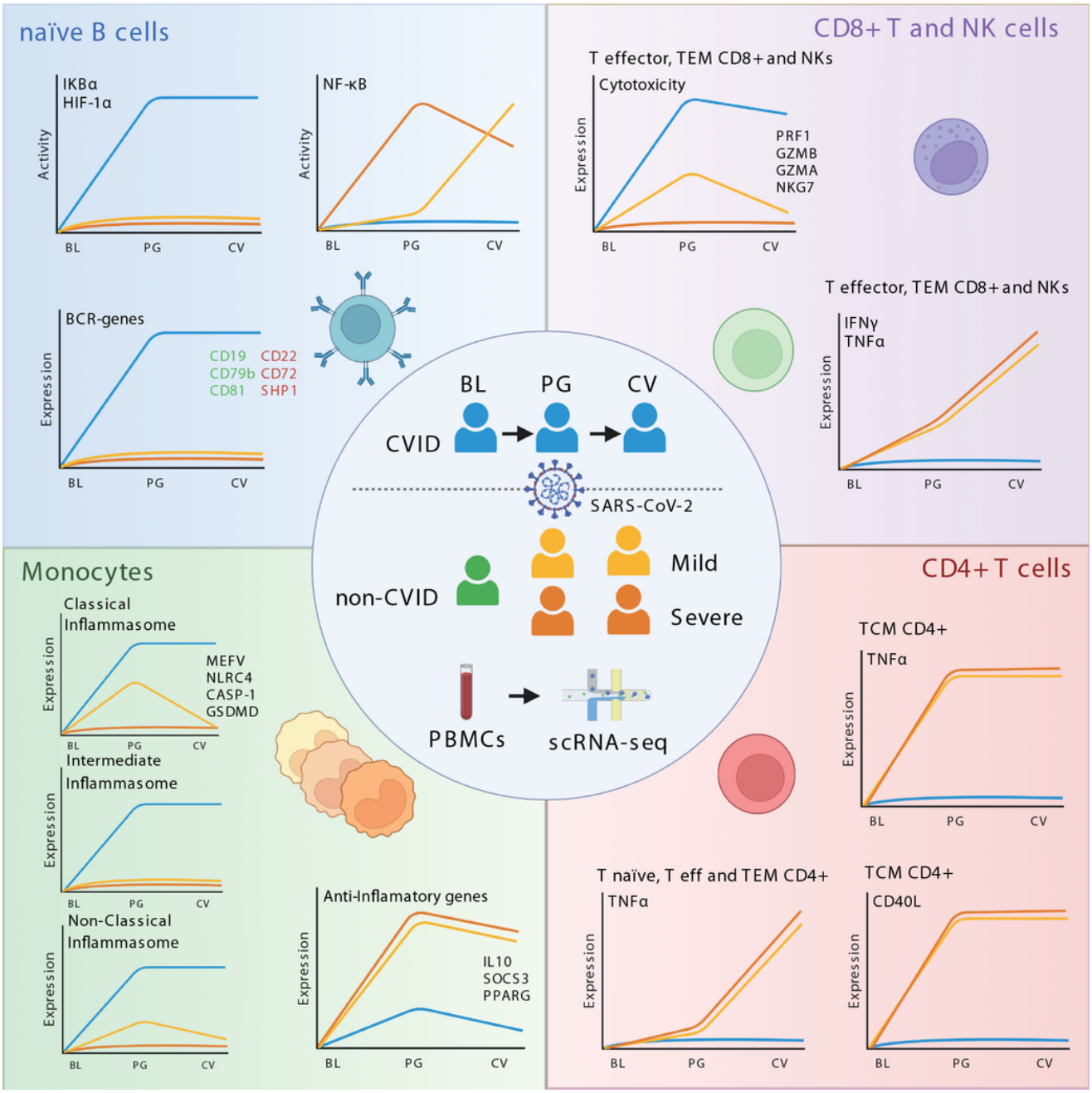

Figure 5

Overview of the dysregulated immune responses in COVID-19 CVID patients. Scheme depicting the altered immune responses in naïve B cells, T and NK cells, as well as monocytes in CVID patients upon SARS-CoV-2 infection and recovery.

Supplementary Files

This is a list of supplementary files associated with this preprint. Click to download.

- SupplementaryTable1.xlsx
- SupplementaryTable2.xlsx
- SupplementaryTable3.xlsx
- SupplementaryFigureLegends.docx
- SupplementaryFigure1.pdf
- SupplementaryFigure2.pdf
- SupplementaryFigure3.pdf